ISEV

Comparing digital detection platforms in high sensitivity immune-phenotyping of extracellular vesicles

Roberto Frigerio[1] | **Angelo Musicò[1]** | **Alessandro Strada[1]** | **Greta Bergamaschi[1]** |
Stefano Panella[2] | **Cristina Grange[3]** | **Marcello Marelli[1]** | **Anna M. Ferretti[1]** |
Gabriella Andriolo[2] | **Benedetta Bussolati[4]** | **Lucio Barile[2]** ⬥ | **Marcella Chiari[1]** |
Alessandro Gori[1] | **Marina Cretich[1]** ⬥

[1]Istituto di Scienze e Tecnologie Chimiche "Giulio Natta" (SCITEC) - Consiglio Nazionale delle Ricerche, Milano, Italy

[2]Istituto Cardiocentro Ticino, Ente Ospedaliero Cantonale, Lugano, Switzerland

[3]Department of Medical Sciences, University of Turin, Turin, Italy

[4]Department of Molecular Biotechnology and Health Sciences, University of Turin, Turin, Italy

Correspondence
Marina Cretich, Istituto di Scienze e Tecnologie Chimiche "Giulio Natta" (SCITEC) - Consiglio Nazionale delle Ricerche, Milano, Italy.
Email: marina.cretich@cnr.it

Alessandro Gori, Istituto di Scienze e Tecnologie Chimiche "Giulio Natta" (SCITEC) - Consiglio Nazionale delle Ricerche, Milano, Italy.
Email: alessandro.gori@cnr.it

Abstract

Despite their clinical potential, Extracellular Vesicles (EVs) struggle to take the scene as a preeminent source of biomarkers in liquid biopsy. Limitations in the use of EVs origin from their inherent complexity and heterogeneity and from the sensitivity demand in detecting low to very low abundant disease-specific sub-populations. Such need can be met by digital detection, namely capable to reach the single-molecule sensitivity. Here we set to compare, side by side, two digital detection platforms that have recently gained increasing importance in the field of EVs. The platforms, both commercially available, are based on the principles of the Single Particle Interferometric Reflectance Imaging Sensing (SP-IRIS) and the Single Molecule Array technology (SiMoA) respectively. Sensitivity in immune-phenotyping of a well characterized EV sample is reported, discussing possible applicative implications and rationales for alternative or complementary use of the two platforms in biomarker discovery or validation.

KEYWORDS
digital detection, extracellular vesicles, liquid biopsy, immunoassays

1 | INTRODUCTION

Extracellular Vesicles (EVs) represent one among the widest biomarker space in the liquid biopsy paradigm, given their ubiquitous distribution within biofluids. The multiple and variegated roles of EVs in intercellular communication have indeed been proposed as pivotal in the pathogenesis and spread of many diseases (Kalluri & LeBleu, 2020; Liang et al., 2021; Yates et al., 2022), including neurodegeneration, tumours and infectious diseases. On the other hand, EVs represent analytes of unprecedented complexity given the heterogeneity of EV sub-populations in terms of cellular origin, biogenesis, molecular composition, structure and function (Bordanaba-Florit et al., 2021; Jeppesen et al., 2019). As such, their comprehensive biological assessment

demands an orchestra of complementary and orthogonal analytical techniques, ranging from 'bulk' characterisations (Hartjes et al., 2019) to single vesicle techniques (Bordanaba-Florit et al., 2021; Hilton & White, 2021).

In this scenario, the hoped-for translation of EV-based systems towards minimally invasive diagnostic practices must also comply with the putative clinical value of low to very low abundant EV sub-types within complex media. In this regard, the enormous diagnostic potential of EVs could be unleashed by the sensitivity provided by digital biosensing platforms, namely capable of reaching the single molecule detection level (Cohen & Walt, 2019; Cretich et al., 2015; Gorris & Walt, 2010)

Oppositely to analogue detection, where the measured signal (mediated by a reporter) is averaged and proportional to the concentration of the bio-species being analysed, in digital detection techniques the signal arises from the measurement of single discrete molecular interaction events (defined as *counts*) rather than from an ensemble readout. To this purpose, the sampling area is uniformly divided into multiple discontinuous compartments to detect the presence or absence (1 or 0) of a single count. In this sense, different approaches were exploited for analytes confinement propaedeutic to their digital counting, including nanodroplets, nanopores, microfluidics, sparse layers and microwells (Cretich et al., 2015; Liu & Lei, 2021). Being less prone to noise than measurement of bulk quantities (Cretich et al., 2015) digital counting of bio-interactions can be exquisitely precise and quantitative, also providing a wider dynamic range of detectable target concentrations and unmatched sensitivity compared to ensemble measurements (Cohen & Walt, 2019; Cretich et al., 2015). As far as coupling to digital readout of EV immune-phenotyping (i.e., characterisation of EV surface molecules by specific antibodies) is concerned, two platforms are finding their place under the spotlight: the ExoView Analizer (https://www.nanoviewbio.com) which is based on the principle of Single Particle Interferometric Reflectance Imaging Sensing (SP-IRIS) (Yurt et al., 2021) and the Quanterix Simoa Technology (https://www.quanterix.com/simoa-technology) based on the Single Molecule Array technology (SiMoA) (Rissin et al., 2010). Both techniques indeed deliver immunoassays with digital readout enabled by single particle confinement, either on sparse layers (spots) in SP-IRIS and in microwells for SiMoA. While these platforms were not originally intended for EV analysis, that is, for label-free virus detection (Daaboul et al., 2014; Rissin et al., 2010; Yurt et al., 2021) (SP-IRIS) and for protein analysis in serum (Rissin et al., 2010) (SiMoA), both systems are currently mature, commercially available technologies used in the context of EVs towards biomarker discovery and validation.

Herein, we set to provide an informative side by side multiparametric comparison of the two platforms which take into account some of the most sought-for features towards EVs translation into the clinics. We critically analysed results and highlighted the most peculiar traits for each system. Finally, we thoroughly discuss possible applicative implications, suggesting rationales for their alternative or complementary use.

Whether imaging (nano)flow cytometry could be assimilated for similar scopes, it will not be included in this comparison and is reviewed elsewhere (Arab et al., 2021; Bordanaba-Florit et al., 2021).

2 | MATERIALS AND METHODS

2.1 | Materials and reagents

Monoclonal antibodies anti-CD9 (clone SN4), anti-CD63 (clone AHN16.1) and anti-CD81 (clone 1.3.3.22) either unconjugated or biotin-labelled are from Ancell Corporation, (Bayport, MN, USA).

Bare silicon chips and Tetraspanin Kits (were provided by NanoView Biosciences (Boston MA). MCP-2 copolymer for chip coating was obtained from Lucidant Polymers (Sunnyvale, CA, USA). Other chemicals were from Sigma-Aldrich (St. Louis, MO, USA) if not stated otherwise.

2.2 | CPCs isolation and culture

Cardiac mesenchymal cardiac-derived cells (namely CPCs) were obtained from atrial appendage explants of patients subjected to valve repair surgery, without any concomitant coronary artery disease. Connective tissue was removed and myocardium minced in small fragments. Tissue fragments were placed in 115 cm^2 tissue-culture flasks (TPP, Switzerland) coated with CELLstart CTS (Gibco/Thermo Fisher Scientific). Tissue-explants were cultured in StemMACS-MSC expansion Media kit XF (Miltenyi Biotec GmbH, Germany).

Outgrowing cells from explants were harvested using TrypLE Select Enzyme (Gibco/Thermo Fisher Scientific), then seeded at $8–10 \times 10^4$ cells/cm^2 and expanded in T flasks (75–150 cm^2) and HYPERFlask (1720 cm^2) culture vessels (Corning). CPCs expanded up to culture passage 4 (P4) were washed twice with DPBS and incubated at 37°C with 5% CO$_2$ in Dulbecco's Modified Eagle Medium (DMEM) 4.5 g/l glucose without phenol red (Gibco/Thermo Fisher Scientific). After about 2 weeks of cell culture, the conditioned medium (CM) containing EVs was harvested.

2.3 | EVs isolation by Tangential Flow Filtration (TFF)

EVs were isolated from media conditioned (CM) by CPC as described by Andriolo et al. (2018). Briefly, CPCs (70%–80% confluent) were washed twice with DPBS and incubated at 37°C with 5% CO_2 in DMEM 4.5 g/l glucose without phenol red (Gibco/Thermo Fisher Scientific). After 7 days, the CM was clarified by 0.22 μm filtration through bottle filter units or on-line filters (ULTA Capsule HC, KMP-HC9202HH, GE Healthcare, USA). Concentration and EV size selection were performed by tangential flow filtration (TFF), using the ÄKTA flux 6 system (GE Healthcare) equipped with a 300 kDa cut-off hollow fiber cartridge (GE Healthcare), the concentration was followed by diafiltration in five volumes of Plasma-Lyte A solution.

2.4 | HeLa and HEK culture and EVs isolation

HEK 293 human cell line (ATCC) was culture using Dulbecco's Modified Eagle Medium (DMEM) 4.5 g/l glucose (Gibco/Thermo Fisher Scientific) supplemented with 10% Fetal Bovine Serum FBS (Gibco/Thermo Fisher Scientific), 1x MEM Non-Essential Amino Acids Solution (NEAA), 100 units/ml of penicillin and 100 μg/ml of streptomycin.

HeLa human cell line (ATCC) was culture using Iscove's Modified Dulbecco's Medium (IMDM) (Gibco/Thermo Fisher Scientific) supplemented with 10% Fetal Bovine Serum FBS (Gibco/Thermo Fisher Scientific), 100 units/ml of penicillin and 100 μg/ml of streptomycin.

Both cell lines were expanded in a T150 flask (TPP Techno Plastic Products), after reaching confluence, cells were washed two times with DPBS and incubated at 37°C with 5% CO_2 in Dulbecco's Modified Eagle Medium (DMEM) 4.5 g/l glucose without phenol red (Gibco/Thermo Fisher Scientific). After 1 week of cell culture, the conditioned medium (CM) containing EVs was harvested and centrifuged at 3000 × g for 20' at 10°C to eliminate larger debrees, and 10,000 × g for 15' at 10°C to deplete larger vesicles. CM was then concentrated using Amicon Ultra Centrifugal Filters (MERK Millipore) equipped with a 30 kDa cut-off filter.

2.5 | Nanoparticle tracking analysis

Nanoparticle tracking analysis (NTA) was performed according to the manufacturer's instructions using a NanoSight NS300 system (Malvern Technologies, Malvern, UK) configured with a 532 nm laser. CPC-EVs were diluted in filtered PBS to a final volume of 1 ml. Ideal measurement concentrations were found by pre-testing the ideal particle per frame value (20–100 particles/frame). The following settings were adjusted according to the manufacturer's software manual. A syringe pump with constant flow injection was used and three videos of 60 s were captured and analysed with NTA software version 3.2. From each video, the mean, mode, and median EVs size was used to calculate samples concentration, expressed is nanoparticles/ml.

2.6 | BCA assay

EV samples and BSA standards for calibration curve were diluted in BCA solution (Pierce BCA Protein Assay Kit, Thermo Fisher Scientific, Rockford, USA) in 1:9 ratio and incubated for 30 min at 37°C. Samples were analysed by a spectrophotometer (HiPo MPP-96 Microplate Photometer, Biosan, Riga, LV) at 562 nm wavelength.

2.7 | Western blotting

5X Laemmli buffer was added to EVs and sample boiled for 5 min at 95°C. Specifically, 10 μg of EVs' proteins (determined by BCA assay) were prepared in non-reducing conditions for tetraspanins detection, while 10 μg were used for ALIX and TSG101 detection. Proteins were separated by SDS-PAGE (4%–20%, Mini-Protean TGX Precast protein gel, Bio-Rad) and transferred onto a nitrocellulose membrane (BioRad, Trans-Blot Turbo). Nonspecific sites were saturated with a TBS-T solution with 1% BSA for 1 h. Membranes were incubated overnight at 4°C with anti-CD9 (1:1000, BD Pharmingen, San Jose, CA, USA), anti-CD63 (1:1000, BD Pharmingen), anti-Alix (1:1000, Santa Cruz, CA, USA), and anti-TSG101 (1:1000, Novus Bio, Centennial, CO, USA). After washing with TBS-T, membranes were incubated with horseradish peroxidase-conjugated (Jackson ImmunoResearch, Tucker, GA, USA) secondary antibodies diluted 1:3000 in TBS-T with 1% BSA for 1 h. After washing, the signal was detected using Bio-Rad Clarity Western ECL Substrate (Bio-Rad) and imaged using a Chemidoc XRS+ (BioRad).

2.8 | Dot blot analysis

3uL of pure sample was dropped off on nitrocellulose membrane (Protran BA 85 Nitrocellulose, 0.45um, Whatman, Germany), three replicants for each sample was done on different nitrocellulose strips. After 15 minutes of drying at room temperature, the membranes were blocked with 5% of BSA in TBS containing 0.05% of Tween 20 (TBS-T), for 1 hour. The membranes were washed three times with TBS-T, and each strip was incubated with an anti-tetraspanin primary antibodies diluted in TBS-T with 1% BSA, Anti-CD9 (BD Pharmingen, 1:1000 dilution), Anti-CD63 (BD Pharmingen, 1:1000 dilution) and Anti-CD81 (Santa Cruz, CA, USA, 1:400 dilution), for 1 hour on orbital shaker. Strips were washed 5 min, for three times with TBS-T, after membranes were incubated with horseradish peroxidase-conjugated (Jackson ImmunoResearch, Tucker, GA, USA) secondary antibodies diluted 1:3000 in TBS-T with 1% BSA for 1 h. Final washers were performed, the signal was detected using Bio-Rad Clarity Western ECL Substrate (Bio-Rad) and imaged using a Chemidoc XRS+ (BioRad).

2.9 | Transmission electron microscopy

Transmission Electron Microscopy (TEM) images were taken by ZEISS Libra 200FE, equipped with a 200kV FEG and a second generation Omega filter. The sample was prepared placing a carbon/formvar TEM grid on a drop EV solution. Then, the drop was blotted and the grid was put on the Uranyl less (EMS-Electron Microscopy Science) straining and then blotted again. The vesicle sizes were measured by iTEM Imaging platform (Olympus).

2.10 | Super resolution microscopy

Super-resolution microscopy acquisition of EVs was performed using Nanoimager S Mark II microscope from ONI (Oxford Nanoimaging, Oxford, UK) equipped with a 100x, 1.4NA oil immersion objective, an XYZ closed-loop piezo 736 stage, and triple emission channels split at 640, 488 and 555 nm. The experiments were performed using EV profiler Kit (ONI) following manufacturer's protocol. Fluorescent antibodies anti CD9-488, CD63-568 and CD81-647 were included in the kit. Images were performed in dSTORM mode acquired sequentially in total reflection fluorescence (TIRF) mode. Single-molecule data was filtered using NimOS software (v.1.18.3, ONI). Data has been analysed with the Collaborative Discovery (CODI) online analytic platform www.alto.codi.bio from ONI and the drift correction pipeline version 0.2.3 was used. (Skovronova et al., 2021)

2.11 | Antibody microarrays for EVs

Silicon chip, with 80 nm oxide layer, were coated with MCP-2 polymer (Lucidant Polymers). The microarrays were produced using a non-contact S12 Spotter (Scienion Co., Berlin, Germany), depositing a drop for each spot (400 pL). Final concentration of antibodies spot solution is 1 mg/ml in PBS and 50 mM Trehalose. Printed chips were placed in humid chamber overnight at room temperature and subsequently were washed in a blocking solution (ethanolamine 50mM, Tris HCl 0.1 M, pH 9).

EV samples were diluted in filtered PBS and incubated on chips for 2 h at room temperature in static conditions. Chips were then placed in a 24 wells plate where 1 ml of filtered PBS was added in each well. Plate was incubated on an orbital shaker at 300 rpm for 3 min, 750 μl of PBS were removed and replaced with fresh PBS. Chips were washed three times and dried.

Chips were then incubated with fluorescent antibodies, (monoclonal anti-CD81, anti-CD63, anti-CD9 from Ancell) in house labelled by Cyanine5 NHS ester from Biotium. Fluorescent antibodies were diluted in filtered incubation buffer (0.05M Tris HCl, pH 7.6, 0.15M NaCl and 0.02% tween 20), 1:1000 ratio and 1 ml added in each well, the plate was placed on shaker 1 h at 300 rpm. After immuno-staining incubation chips were washed and dried. The chips were imagined with ExoView R100 reader using nScan software to acquire the data to be analysed by ExoView Analyzer software

2.12 | Beads-antibody conjugation for SiMoA platform

Beads conjugation to antibodies was performed according to Quanterix Homebrew kit instructions using the recommended buffers as follows. Conjugation of 150 μl of carboxylate paramagnetic beads (2.8 × 10^9 prt/ml) are washed three times with 300 μl of Bead Wash Buffer (Quanterix, phosphate buffer with detergent), after every washing step the beads are pulsed spin and placed on a magnetic separator for 1 min to aspirate the supernatant. The beads are washed three more times with 300 μl of Bead Conjugation Buffer (Quanterix, 50 mM MES buffer pH6.2) and then are activated with EDC 0.3 mg/ml for 30 min at 4°C under mixing/shaking.
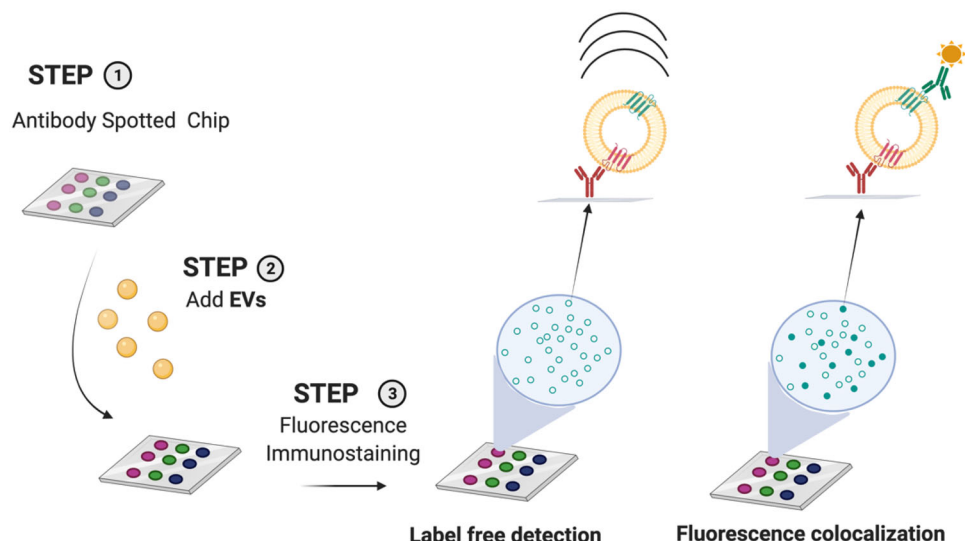
SCHEME 1 Workflow for the analysis of EVs by SP-IRIS. A microchip is arrayed with capturing antibodies, incubated with the EV sample and with fluorescent antibodies. Based on the Single Particle Interferometric Reflectance Imaging Sensing (SP-IRIS) principle, spots are individually imaged to count and size the captured vesicles in a label free fashion. As a further level of characterisation, staining with fluorescent antibodies provide information on the presence and co-localisation of EV associated protein markers. Surface markers as well as internal markers can be detected following specific permeabilisation protocols

Eighty micrograms of antibody (CD9, CD63, CD81) are buffer exchanged with a 50 KDa Amicon filter and antibodies recovered in the Quanterix Bead Conjugation Buffer, after buffer exchange antibody concentration is measured with a Nanodrop spectrophotometer (ThermoFisher) and adjusted to 0.2 mg/ml with Bead Conjugation Buffer.

Three hundred microlitres of a 0.2 mg/ml antibody solution are added to the activated paramagnetic beads and incubated for 2 h at 4°C under mixing/shanking. After the conjugation step the beads are washed two times with Bead Wash Buffer and then are blocked with Bead Block Buffer (Quanterix, phosphate buffer with BSA) for 45 min at room temperature under mixing/shaking. After blocking, beads are washed three times with Bead Diluent and stored until use at 4°C.

2.13 | SiMoA two-step assay

Beads solution are prepared at the concentration of 2×10^7 beads/ml in Bead Diluent. The detector antibody (biotinylated CD9, CD63, CD81 antibodies) solutions (1 μg/ml) are diluted in Homebrew Sample Diluent (Quanterix), similarly, each sample is diluted 1:4 in Homebrew Sample Diluent (Quanterix). Twenty five microlitres of beads are transferred into a 96 microwell plate and mixed with 20 μl of detector antibody and 100 μl of sample. Sample, beads and detector are incubated for 30 min at 25°C at 800rpm. After incubation, beads are washed with an automatic plate-washer and then each incubated for 10 min with a 150 pM SBG solution (in SBG Diluent, Quanterix). After SBG incubation step the plate is washed again by the automatic plate-washer and then inserted into the Quanterix SR-X instrument for analysis where RGP automatically added. Data were analysed and processed by Reader Software SiMoA 1.1.0.

3 | RESULTS

3.1 | Platforms overview

The ExoView Platform entails a microchip-based workflow that integrates two different detection steps (Scheme 1). First, an antibody-spotted chip is incubated with the EV sample followed by individual imaging of single spots to count in a label-free fashion the captured EVs. This step relies on Single Particle Interferometric Reflectance Imaging Sensing (SP-IRIS) (Daaboul et al., 2014): when a LED source illuminates (bio)nanoparticles captured on to the sensor surface (a silicon dioxide layer on top of a silicon substrate), the interference of light reflected from the sensor surface is modified by the presence of particles producing a distinct signal (Yurt et al., 2021) . Besides enabling their single count, the contrast of the detected particles is also used to estimate their size distribution in the 50–200 nm range. Inherently, the bioparticles counting and sizing associated to each spot within the antibody array provides information on their immune-phenotype, as different antibodies can be simultaneously probed as capturing agents (Daaboul et al., 2016). As a further level of characterisation, the immune-staining of captured EVs with fluorescent antibodies is used to obtain additional information on the presence of other protein markers on individually
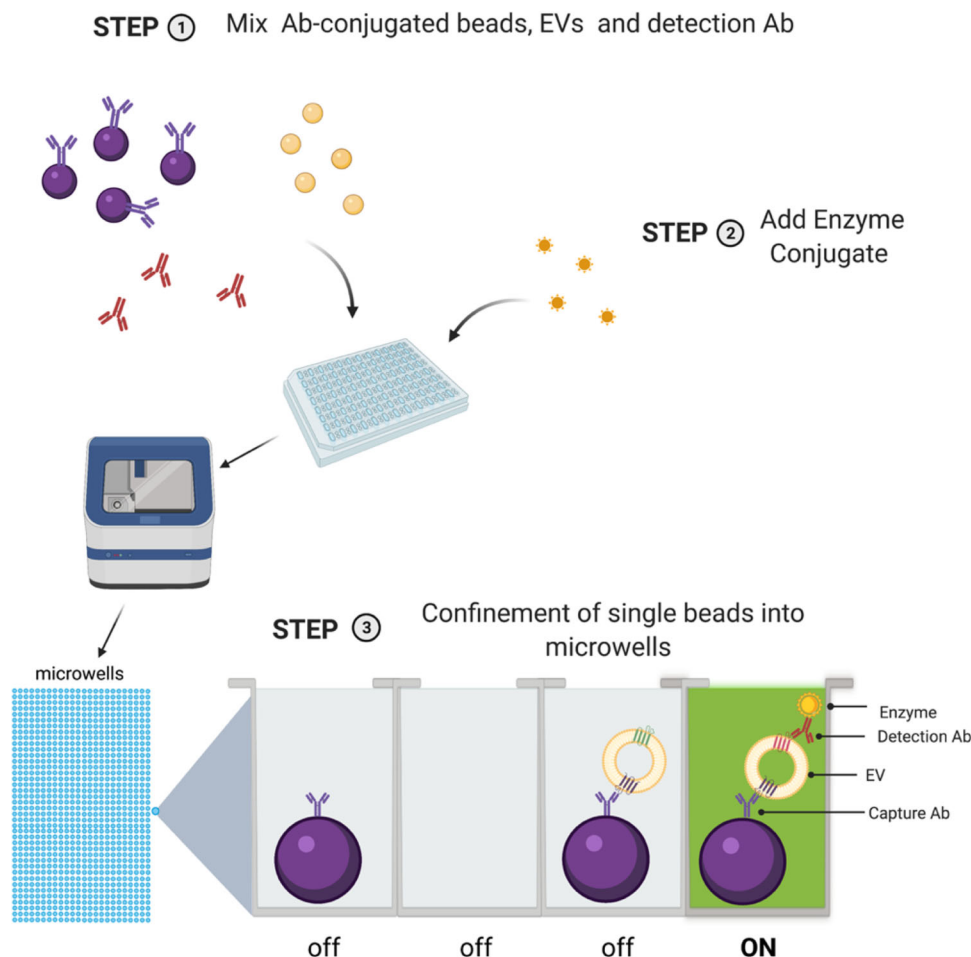
SCHEME 2 Workflow of the analysis of EVs by SiMoA. The EV sample is mixed with antibody-functionalised paramagnetic microbeads and with biotinylated (detector) antibodies in a classical sandwich assay. When enzyme conjugate streptavidin-β-galactosidase (SBG) and fluorogenic substrate resorufin β-D-galactopyranoside (RGP) are added, a fluorescence signal is produced. Beads are distributed over an array of microwells able to confine one single bead each (one bead per well) where the high local concentration of generated fluorophores will ensure a detectable signal even for one captured EV. Fluorescence imaging of the microwell array will distinguish 'on' signals corresponding to labelled beads and 'off' signals corresponding to empty wells or unlabelled beads

captured vesicles in a diverse set of applications (Dogrammatzis et al., 2021; Gori et al., 2020; Khan et al., 2021; Mizenko et al., 2021). Importantly, this enables to quantitatively correlate the simultaneous presence of multiple protein markers on the same particle under analysis (co-localisation), potentially proving of highly informative value.

SiMoA platform, (Simoa Bead Technology), was originally introduced as an immunoassay technology for protein measurements at the single molecule level (Rissin et al., 2010). The test format is a sandwich immunoassay performed on paramagnetic microbeads (3.4 μm) conjugated to a capture antibody (Scheme 2). Detection is allowed by the use of a biotinylated antibody which binds to streptavidin-β-galactosidase (SBG), which acts on the fluorogenic substrate resorufin β-D-galactopyranoside (RGP). Upon incubation of microbeads with the EV sample, the detection cocktail is added, beads are then distributed over an array of microwells, each one able to confine a single microbead. Due to the low (femtolitre) volume of microwells, the high local concentration of generated fluorophores will ensure a detectable signal even for one captured target entity. By acquiring fluorescence images of the array, it is possible to distinguish 'on' signals corresponding to labelled beads (where EVs are sandwiched between capture and detection antibodies) and 'off' signals corresponding to empty wells or unlabelled beads (Scheme 2).

SiMoA was recently applied to the detection of EVs for the liquid biopsy of colorectal cancer (Wei et al., 2020), large B cell lymphoma (Li et al., 2021), breast cancer (Morasso et al., 2022), proposed to study the association of the neuronal marker L1CAM to EVs (Norman et al., 2021) and compare different EV isolation protocols (Ter-Ovanesyan et al., 2021).

3.2 | EV sample characterisation

EVs from human cardiac progenitor cells (CPCs) used in this study were produced according to a previously devised GMP-grade manufacturing protocol (Andriolo et al., 2018). This is a standardised and relatively large scale production method providing
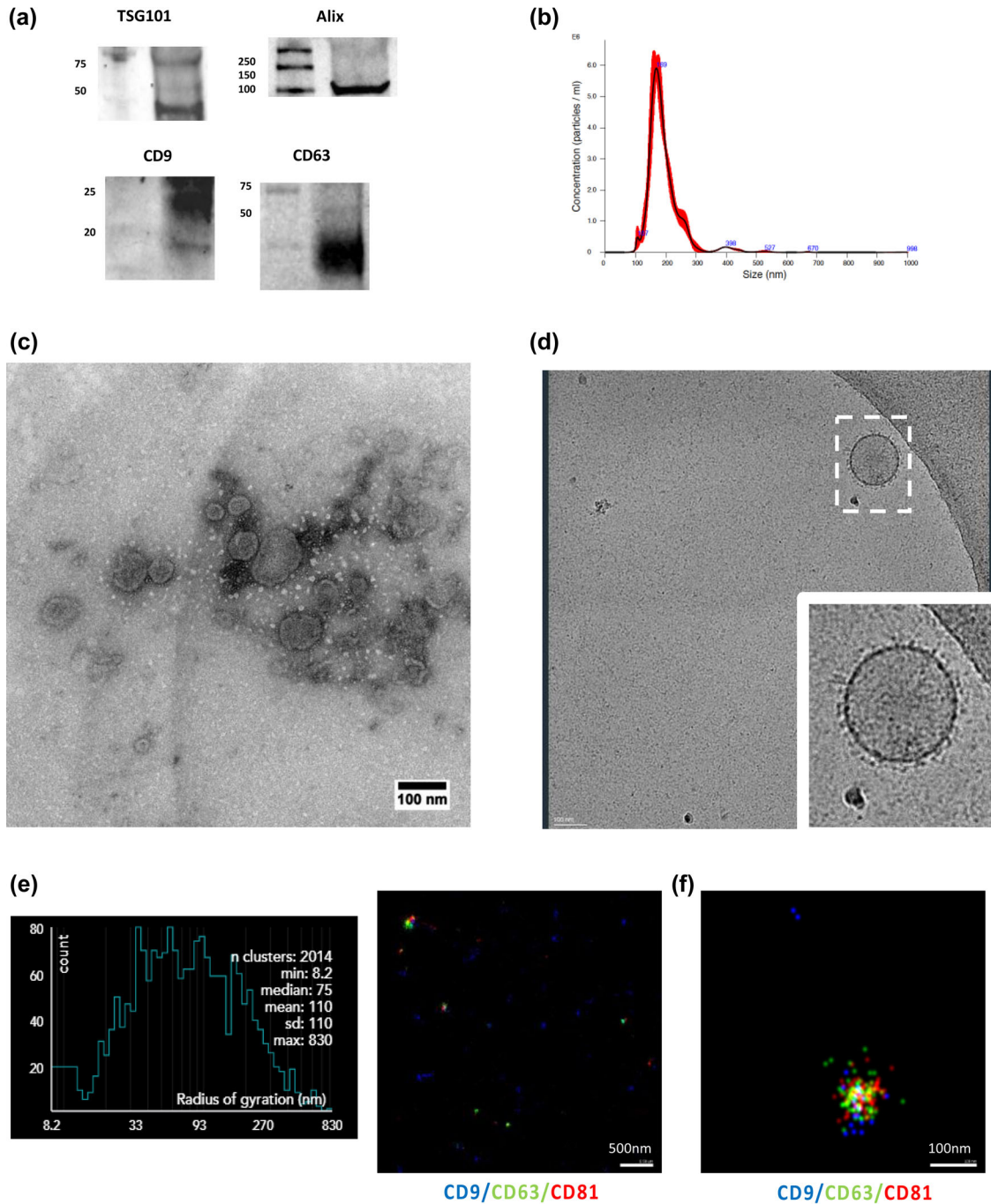
FIGURE 1 Characterization of EVs from human Cardiac Progenitor Cells (CPCs). a) Western Blotting (WB) to confirm the presence of luminal markers Alix and TSG101 and transmembrane proteins CD9 and CD63. b) Nanoparticle Tracking Analysis (NTA) quantification and size distribution of particles contained in the sample. A mean particle size of 193 ± 2 nm and a concentration of 4.56×10^{10} particles/ml was found. c) Imaging by Transmission Electron Microscopy (TEM) showing a heterogeneous preparation of EVs with dimensions around 100 nm and lower. d) Cryo-Electron Microscopy visualisation of the sample highlights some of the typical features of EVs such as a regular round shape, a lipid bilayer/membrane surrounded by electron-dense material and an electron dense cargo lumen. e) Representative graph of EV size distribution obtained with SRM. f) Representative SRM images of CPC - EVs stained with tetraspanins (CD63: green, CD81: red and CD9: blue), left panel: 500 nm magnification, right panel: 100 nm magnification

EV batches large enough to run all sample characterisations and replicate experiments needed for comparing the two platforms, thus avoiding batch-to-batch variations.

According to MISEV guidelines (Théry et al., 2018) the CPCs-EV sample was characterised by Western Blotting (WB), NTA, TEM, Cryo-Electron Microscopy (Cryo-EM) and Super Resolution Microscopy. Results confirmed the presence of vesicles with size, morphology and protein content compatible with EVs as shown in Figure 1. Quantification and size distribution of particles

were analysed by NTA (Figure 1b) providing a mean particle size of 193 ± 2 nm and a concentration of 4.56×10^{10} particles/ml. Of note, a remarkable difference in size distribution was observed in characterising EVs by microscopy techniques. TEM (Figure 1c) indeed showed the presence of a heterogeneous population of EVs with dimensions around 100 nm and lower, that were further visualized by Cryo-Electron Microscopy (Figure 1d), highlighting typical features of EVs such as regular round shape, the presence of a lipid bilayer/membrane surrounded by electron-dense material and an electron dense cargo lumen. Using Super Resolution Microscopy (SRM) based on tetraspanin staining, the size of tetraspanin-positive CPC EVs was quantified as around 75 ± 11 nm median and 110 ± 6 nm mean, in good accordance with Cryo EM and TEM analysis. As previously reported (Cavallaro et al., 2021; Skovronova et al., 2021; van der Pol et al., 2014; Welsh et al., 2020) the overestimation of EV diameter by NTA could be ascribed to EV aggregation or, most likely, to instrument inability to detect EVs smaller than 70 nm. A further explanation could be the evaluation of the EV hydrodynamic size under solution using NTA, in comparison with the measurement of the dry radius with microscopy techniques (Montis et al., 2017).

The presence of luminal markers Alix and TSG101 and transmembrane proteins CD9 and CD63 were confirmed by WB (Figure 1a). In our hands CD81 was not detectable by WB, however a faint signal was visible by Dot Blot analysis (Figure S1). Super Resolution Microscopy with CD9/CD81/CD63 fluorescence staining confirmed the presence of all three surface markers, being EVs positive for single, double, triple markers (Figure 1f).

3.3 | EV phenotyping assays

It is well-known that tetraspanins are not ubiquitously and homogeneously expressed on EVs (Campos-Silva et al., 2019; Mizenko et al., 2021; Yoshioka et al., 2013). However, transmembrane proteins CD9, CD63 and CD81 are to date considered amongst the more represented and typical EV markers and, as such, widely used for relative quantification of EVs (Théry et al., 2018). As model surface markers to compare the two analytical platforms, we thus focused our study on their immune-phenotyping by sandwich immunoassays. To this aim, monoclonal antibodies (mAb) anti-CD9 (clone SN4), anti-CD63 (clone AHN16.1) and anti-CD81 (clone 1.3.3.22) were selected and, for a fair comparison of data, applied to both SP-IRIS and SiMoA platforms by developing custom functionalisation of chips and beads respectively. Being EVs multi-marker analytes, where multiple copies of the same protein are likely exposed on the membrane of the same vesicle, each antibody clone can be simultaneously used both as capture and detection agent in a sandwich immunoassay.

For the SP-IRIS experiments, microarray chips were spotted with individual anti CD9, CD63 and CD81 mAbs and with a solution containing a 1:1:1 mixture of the three clones. We devised two detection formats (Scheme 3). In the 'Single-tetraspanin' detection, EVs were captured on spots by an individual anti-tetraspanin mAb, and subsequently revealed by the same fluorescence-labelled mAb providing information on single tetraspanin phenotype (assays StCD9, StCD63, StCD81).

In the design of the SiMoA experiments (Scheme 4) the same rational was applied: capturing beads were separately functionalized with anti CD9, CD63 and CD81 mAbs and with a 1:1:1 mixture of the three mAbs. In the 'Single-tetraspanin' detection, after EV capturing on each bead type, single biotin labelled versions of a mAb were used individually for detection (assays StCD9, StCD63, StCD81).

In the 'Pan-tetraspanin' detection scheme, the EVs captured on the four bead types were detected by a mixture of the three labelled mAbs (assays PtCD9, PtCD63, PtCD8, PtMix).

3.4 | SP-IRIS assays

Bare silicon chips for SP-IRIS were coated by MCP2 polymer and spotted with tetraspanin antibodies according to previously devised protocols (Daaboul et al., 2016; Frigerio et al., 2021; Gori et al., 2020). Chips were incubated with various amounts of CPCs - EVs ranging from 0 to 10^{10} vesicles/ml according to NTA determination. Even if NTA cannot be considered accurate in defining the absolute concentration of EVs in solution, we used the particle determination by NTA to express EV concentration, estimate indicative detection ranges and to normalise the data obtained in comparing the two platforms.

Following washing steps, the 'Single-tetraspanin' and the 'Pan-tetraspanin' detection schemes were applied (Scheme 3). The fluorescent particle counts detected by ExoView R100 platform for the 'Single tetraspanin' protocol for EVs ranging from 10^5 to 10^{10} particle/ml are reported in Figure 2, left panel, whereas the right panel shows results for the 'Pan-tetraspanin' detection mode. For both protocols, a $10^8 - 10^{10}$ particles/ml detection range is observable, with differences among curves ascribable to several factors including the differential level of tetraspanin expression in the CPC-EV sample and differences in mAb affinity. Notably, the use of a mixture of the three mAbs either in the capturing spot and/or in the detection cocktail (Pan-tetraspanin assay) generally did not provide noticeable advantages in terms of limits of detections (LODs), that vary from 10^6 to 10^9 EV/ml, depending on the assay (Table 1). For evaluation of the EV LODs in all tested conditions we considered the lowest EV concentration providing a fluorescence signal that, according to the Student's t test, was assessed as statistically different ($p < 0.05$) from the background (signal detected for the blank sample) (Figure S2 and S3).
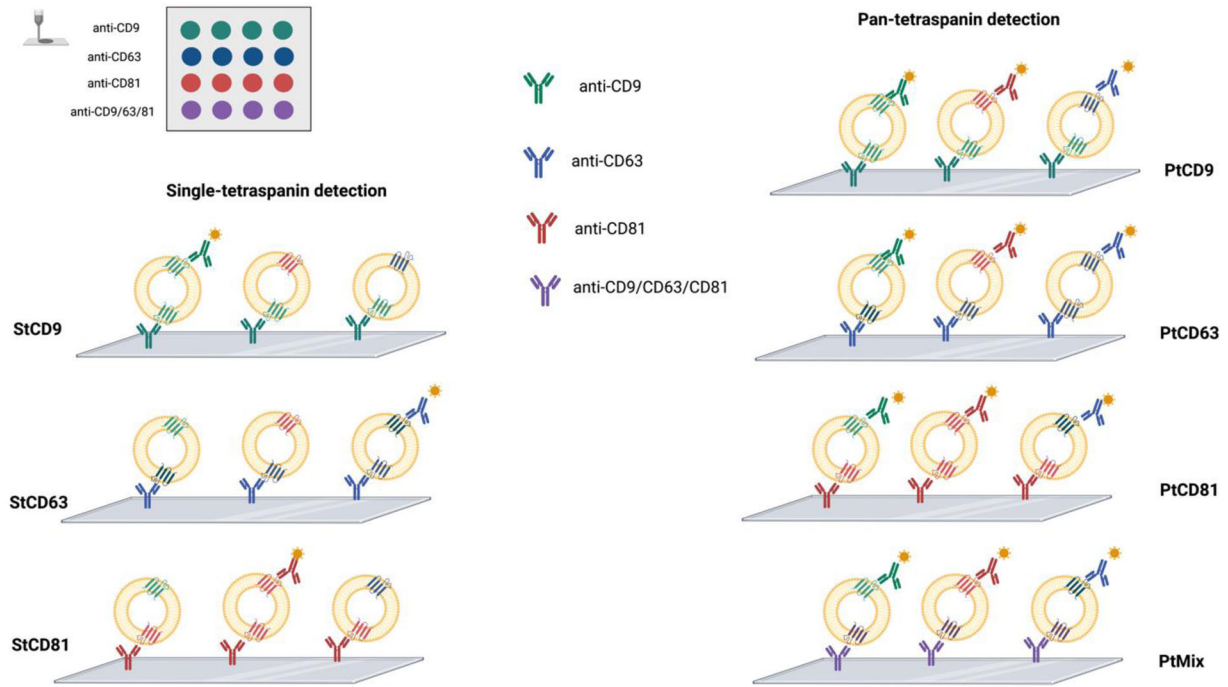
SCHEME 3 CD9, CD63 and CD81 phenotyping on SP-IRIS. Microarrays were spotted with anti CD9, CD63, and CD81 antibodies and with a solution containing a 1:1:1 mixture of the three clones. In the 'Single-tetraspanin' detection (left panel), EVs were captured and then revealed by the same fluorescence-labelled mAb (assays StCD9, StCD63, StCD81). In the Pan-tetraspanin detection (right panel), EVs were captured either by individual anti-tetraspanin mAb of by a mixture of the three clones. Microarrays were then incubated by a cocktail of the three fluorescent antibodies (assays PtCD9, PtCD63, PtCD8, PtMix)
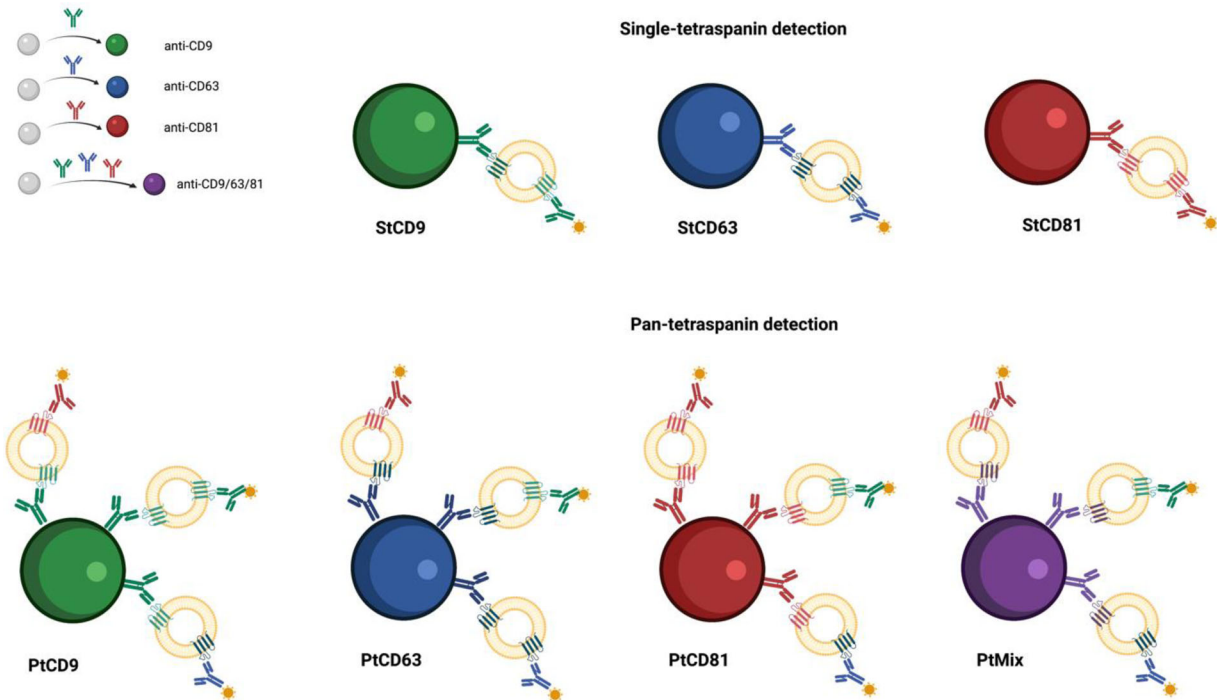
SCHEME 4 CD9, CD63 and CD81 phenotyping on SiMoA. Capturing beads were functionalised with anti CD9, CD63 and CD81 antibodies and with a 1:1:1 mixture of the three. In the Single-tetraspanin detection (upper panel), after EV capturing, single biotin labelled versions of a tetraspanin antibody were used individually (assays StCD9, StCD63, StCD81). In the Pan-tetraspanin detection scheme (lower panel), the EVs captured on the four bead types are labelled by a mixture of the detection antibodies (assays PtCD9, PtCD63, PtCD8, PtMix)
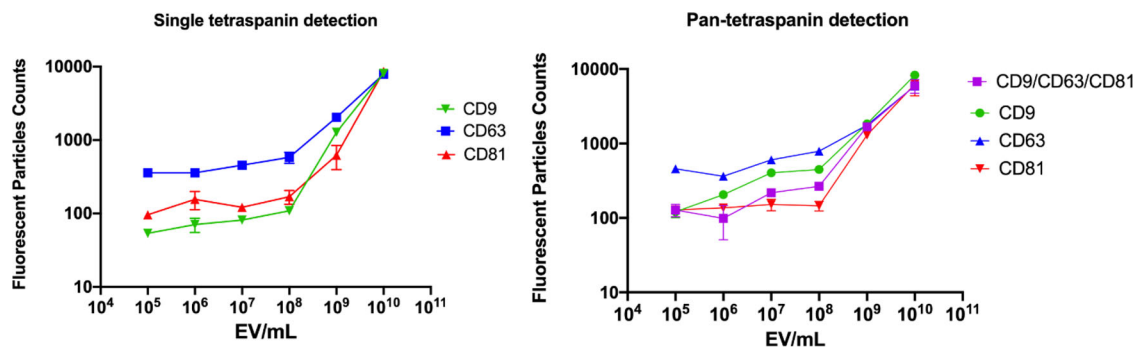
FIGURE 2 Fluorescent particle counts detected by SP-IRIS through the ExoView R100 platform for the CPCs derived EVs sample ranging from 10^5 to 10^{10} particle/ml. Left panel: results for the 'Single tetraspanin' protocol, right panel: results for the 'Pan-teraspanin' detection mode. Data were obtained from two biological replicates

TABLE 1 Limits of Detection (LODs) for the SP-IRIS platform calculated considering the lowest EV concentration providing a fluorescence signal significantly ($p < 0.05$) different from blank sample (Figure S2 and S3)

Assay	Single tetraspanin detection	Assay	Pan-tetraspanin detection
StCD9	10^6 EV/ml	PtCD9	10^6 EV/ml
StCD63	10^8 EV/ml	PtCD63	10^7 EV/ml
StCD81	10^9 EV/ml	PtCD81	10^9 EV/ml
		PtMix	10^8 EV/ml

TABLE 2 Limits of Detection (LODs) for the SP-IRIS platform using ExoView Tetraspanin Kit, calculated considering the lowest EV concentration providing a fluorescence signal significantly ($p < 0.05$) different from blank sample (Figure S6)

Assay	ExoView Tetraspanin Kit
StCD9	10^8 EV/ml
StCD63	10^7 EV/ml
StCD81	10^8 EV/ml

The best sensitivity performance (LOD of 10^6 EV/ml) is obtained with StCD9 and PtCD9 assay suggesting a relative high abundance of CD9 in the analysed sample. To avoid any possible bias in the sensitivity comparison, all experiments were run on the same (red) fluorescence channel.

It is worth noticing that ExoView analyser returns additional information on the sample, including co-localisation of different protein markers on single EVs (when multiple fluorescence channels are used) and, based on the label-free interferometric detection, the size of individual EVs. Figure S3 shows the results of size versus fluorescence intensity of single detected EVs in the 10^9 EV/ml sample analysed by the Single-tetraspanin detection (StCD9, StCD63 and StCD81 assays) which suggests a higher abundance and a slightly lower size of CD9 positive EVs in the CPC derived sample.

The same EV dilution curve was analysed by commercially available ExoView Tetraspanin Kit, which allows for the 'Single-tetraspanin' assay only, with detection on three different fluorescent channels. It is worth underlining that, in terms of comparison with the above reported data, antibody specifications are not disclosed to customers nor it is whether different clones are used for tetraspanin capturing and detection. Results of the analysis of the CPC-EV dilution curve by the commercial kit are reported in SI, (Figures S4 and S5) showing that overall performance in terms of detection range was in line with results obtained by our custom assay. Of note, with the commercial chips, CD9 did not perform as the most sensitive marker, being CD63 the one providing the lowest LOD, equal to 10^7 EV/ml (Table 2). This result questions the hypothesis that CD9 is the more abundant tetraspanin in the analysed sample and rather points towards different affinities of antibodies and/or lower cross-talking as plausible explanations for the different observed sensitivities.

3.5 | SiMoA assay

SiMoA assays were developed according to the Quanterix Homebrew assay instructions as detailed in the Section 2 (same antibodies as in the SP-IRIS assay were used). A two-step assay was optimized (see Section 2) preceding immunocomplexes to be
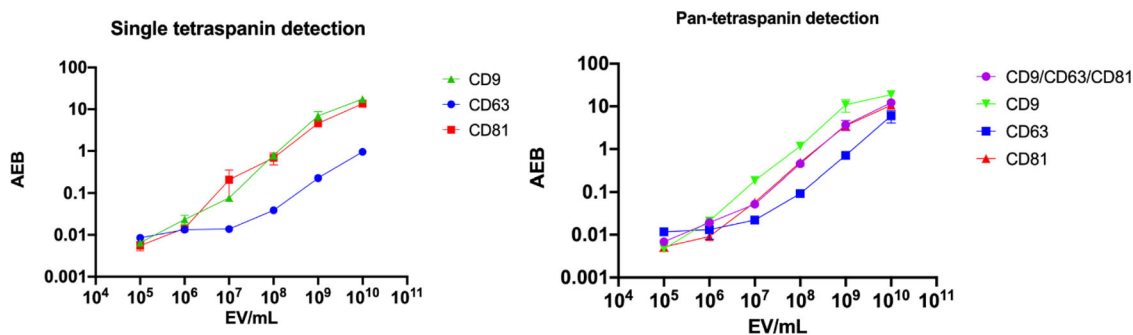
FIGURE 3 SiMoA results of immune-phenotyping of the CPCs derived EVs sample ranging from 10^5 to 10^{10} particle/ml, expressed as Average Enzyme per Bead (AEB) and detected for the Single tetraspanin mode (left panel) and the Pan-tetraspanin mode (right panel). Data were obtained from two biological replicates

TABLE 3 Limits of Detection (LODs) for the SiMoA platform calculated considering the lowest EV concentration providing a fluorescence signal significantly ($p < 0.05$) different from blank sample (Figure S7 and S8)

Assay	Single tetraspanin detection	Assay	Pan-tetraspanin detection
StCD9	10^6 EV/ml	PtCD9	10^5 EV/ml
StCD63	10^6 EV/ml	PtCD63	10^6 EV/ml
StCD81	10^5 EV/ml	PtCD81	10^5 EV/ml
		PtMix	10^6 EV/ml

isolated into femtoliter wells that fit just one bead per well and where antigen-positive vesicles are counted. As previously devised for the SP-IRIS assay, detection was performed in the 'Single-tetraspanin' mode (Scheme 4) and in the 'Pan-tetraspanin' detection mode (Scheme 4). Similarly to SP-IRIS assay, dilution curves of CPCs-EVs ranging from 0 to 10^{10} vesicles/ml were analysed. Results reported in Figure 3, for the analysis of 10^5 to 10^{10} particle/ml range, are expressed as Average Enzyme per Bead (AEB), left panel refers to 'Single tetraspanin detection' detection and right panel to 'Pan-tetraspanin' mode.

For both assay schemes, a $10^5 – 10^{10}$ EV/ml detection range is observable, broader than that observed with the SP-IRIS technique. The limits of detection (LODs) reported in Table 3 were calculated as the lowest concentration assessed by Student's t test as statistically different ($p < 0.05$) from the background signal detected for the blank sample (Figure S7 and S8) and proved to be in the range $10^5–10^7$ EV/ml depending on the assay scheme. The best sensitivity performance (10^5 EV/ml) is obtained with StCD81 assay and PtCD9 and PtCD81 in mixed detection. Again, it is not trivial to determine whether these differences in LODs actually reflect tetraspanins differential abundance rather than antibody affinity.

3.6 | Platforms LODs versus tetraspanin relative expression

In order to correlate the limits of detection obtained by SP-IRIS and SiMoA assays with the relative abundance of CD9/CD63/CD81 measured by an independent technique, we took advantage of Super Resolution Microscopy (SRM). To expand the dataset provided in this comparison, two samples were added to this investigation: EVs isolated from HEK and HeLa cells (see Section 2). Single-tetraspanin assays were performed by SP-IRIS (Scheme 3) and SiMoA (Scheme 4) on serial dilutions of HeLa and HEK derived EVs and compared with CPC-EVs. For SRM experiments, three-colours staining was performed using anti-CD9, anti-CD63 and anti-CD81 fluorescently labelled antibodies and dSTORM single-molecule surface analysis was followed by quantification of tetraspanin expression (absolute number of events is reported in Figure S9). The relative abundance of each marker was calculated as their percentage over total positive events (Figure 4, left panel) and compared with SP-IRIS and SiMoA single-tetraspanin curves (Figure 4, centre and right panel respectively). In all three EV samples, SRM analysis showed CD9 as the most expressed marker (close to be detectable in 100% of all EVs) whereas CD63 and CD81 varied among the samples. CD9 highest abundance is well reflected by the high intensity of SiMoA dilution curves in all three samples. CD63 is less expressed in HEK, which nicely reflects into the lower intensity of the dilution curves for both SP-IRIS and SiMoA, whereas it is more abundant in HeLa EVs, in accordance with SiMoA curves. CD81 is more expressed in CPC-EVs as confirmed by both curves, however the relative differences in the three EV types was reflected only on the SiMoA platform.

The highest abundance of CD9 in all EV types is not always consistent with the lowest LODs (see Tables 4 and 5), in line with the dependence of LODs not exclusively on the relative abundance of the target marker, which defines signal intensity, but by
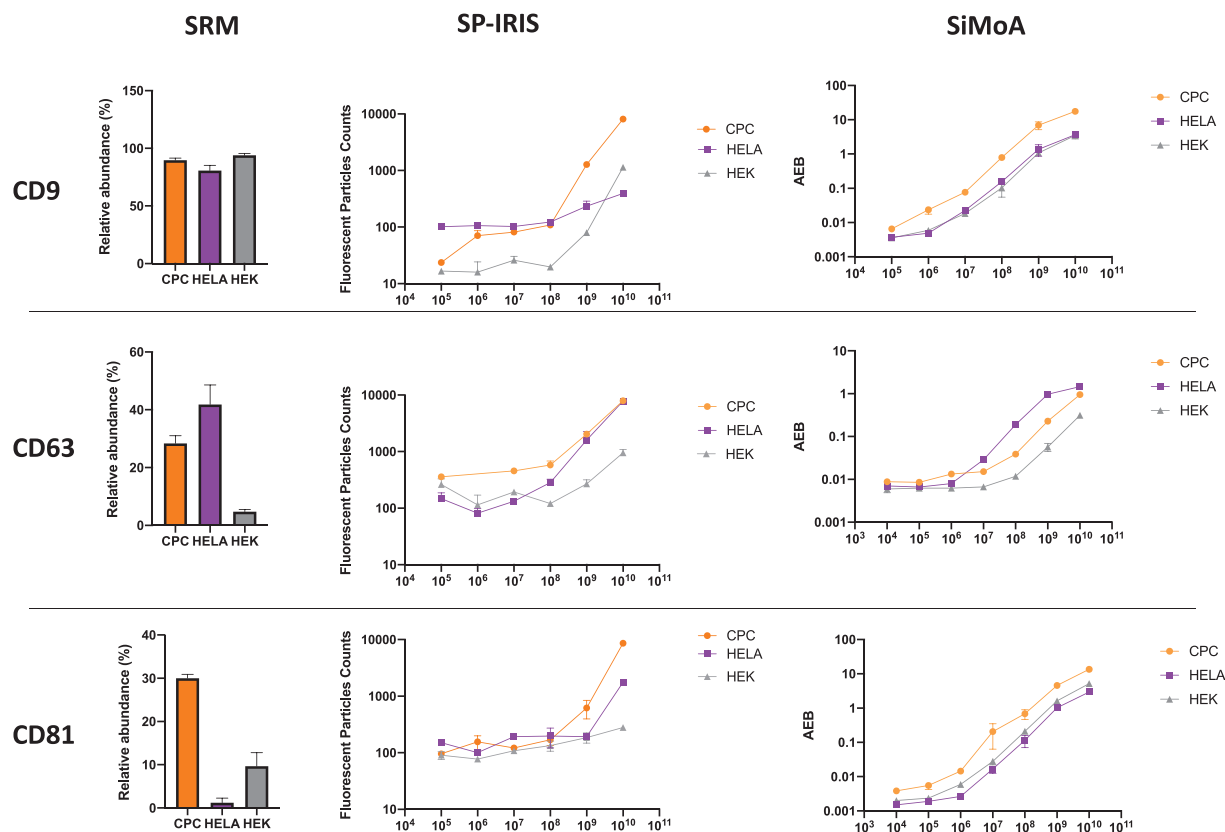
FIGURE 4 Comparison of CD9/CD63/CD81 detection on CPC, HeLa and HEK derived EVs as determined by SRM (left panel), SP-IRIS (central panel) and SiMoA (right panel) following single-tetraspanin assays

TABLE 4 Limits of Detection (LODs) for the SP-IRIS platform (single-tetraspanin assay) calculated considering the lowest EV concentration providing a fluorescence signal significantly ($p < 0.05$) different from blank sample (Figure S10–S12)

SP-IRIS	CPC-EV	HeLa EV	HEK EV
LOD CD9	10^6 EV/ml	10^8 EV/ml	10^9 EV/ml
LOD CD63	10^7 EV/ml	10^8 EV/ml	10^{10} EV/ml
LOD CD81	10^9 EV/ml	10^{10} EV/ml	10^8 EV/ml

TABLE 5 Limits of Detection (LODs) for the SiMoA platform (single-tetraspanin assay) calculated considering the lowest EV concentration providing a fluorescence signal significantly ($p < 0.05$) different from blank sample (Figure S13–S15)

SiMoA	CPC-EV	HeLa EV	HEK EV
LOD CD9	10^6 EV/ml	10^7 EV/ml	10^6 EV/ml
LOD CD63	10^6 EV/ml	10^7 EV/ml	10^7 EV/ml
LOD CD81	10^5 EV/ml	10^6 EV/ml	10^6 EV/ml

noise factors as well, including antibody cross-talk (blank signal) and other sources of background noise. On the other hand, the low expression of CD81 in HeLa and CD63 in HEK is invariably reflected in the corresponding poor LODs found for SP-IRIS (10^{10} EV/ml in both cases) but not in SiMoA, where sensitivity is maintained (10^6 and 10^7 EV/ml). We speculate that this marked difference in the detection of low abundant species could be partially ascribed to the suspension array format, which is more efficient in overcoming the mass-transport limitations that can plague biomolecular interactions at the solution-analytical support interface (Zhao et al., 2010).
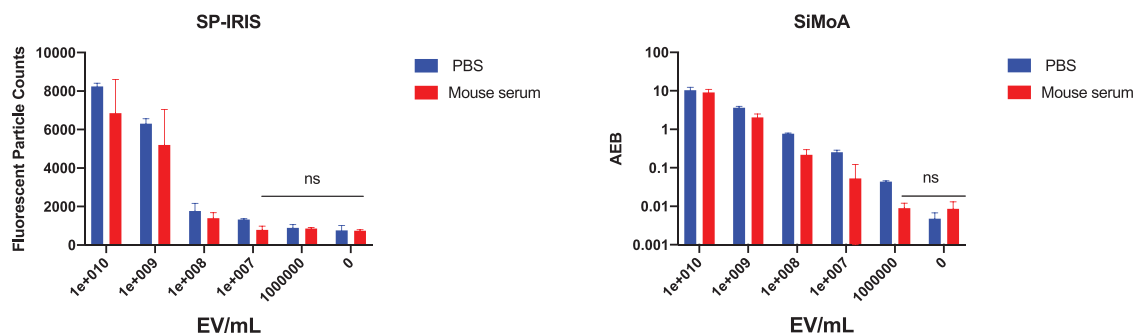
FIGURE 5 Results of immune-phenotyping after spiking human CPCs - EVs into mouse serum and PBS by using the Pan-tetraspanin detection mode. Left panel: fluorescent particle count detected by SP-IRIS. Right panel: Average Enzyme per Bead (AEB) detected by SiMoA platform. *t* test was used to evaluate what is the lowest EV concentration providing a detection signal significantly different from the one provided by the blank sample ($p < 0.05$)

TABLE 6 Lowest detectable concentration of human CPCs - EVs into mouse serum and PBS by the SP-IRIS and SiMoA platforms

	SP-IRIS	SiMoA
PBS	10^7 EV/ml	10^6 EV/ml
Mouse Serum	10^8 EV/ml	10^7 EV/ml

3.7 | Testing recovery in complex samples by spiking assay

High sensitivity detection of minority subpopulations of EVs in biological fluids is pivotal towards EV-based liquid biopsy (Min et al., 2021). Even if EV isolation and enrichment techniques such as ultracentrifugation, size-exclusion chromatography and polymer precipitation can help in yielding more concentrated samples, they also introduce pre-analytical issues such as differential co-isolation of EV subpopulations or interfering contaminants and can affect the surface characteristics of EVs (Tian et al., 2020). In this context, extension of immune-phenotyping of EVs to complex samples would represent a highly desirable step towards 'real life' clinical needs. Here, to promptly compare the two digital platforms, we mimicked a liquid biopsy by spiking the human CPCs - EVs into mouse serum. First we assessed that the tetraspanin monoclonal antibodies used in this work are not cross-reactive to mouse (negligible signals detected for EVs in mouse serum). Then, the 'Pan-tetraspanin' detection scheme was applied both to SP-IRIS and SiMoA platforms. Figure 5 reports the results of the two assays run on the SP-IRIS (left panel) and SiMoA (right panel). EV spiking in PBS and mouse serum were compared. The lowest detectable concentration of CPCs - EVs in mouse serum (signal statistically different from blank) were determined leading to a LOD of 10^8 EV/ml for the SP-IRIS platform and 10^7 EV/ml for the SiMoA instrument (Table 6). In both platforms, sensitivity is affected by sample matrix effect (1 order of magnitude higher LODs compared to spiking in PBS) and face the challenge, typical of blood based liquid biopsy, to detect that small fraction of disease-related EV subpopulation present in the estimated 2×10^{10} EV/ml content in blood (Johnsen et al., 2019).

Taking for granted the selectivity of the antibodies used, we speculate that matrix interfering factors could influence the sensitivity of the techniques together with the presence of typical serum contaminants such as lipoproteins and protein aggregates.

Whether these instrumental capabilities will be enough to provide accurate diagnostic or prognostic information is inherently dictated by the relative abundance of the EV surface marker of interest. In addition, given that tetraspanin CD9/CD63/CD81 are not homogeneously distributed across single EVs (Mizenko et al., 2021; Skovronova et al., 2021), their use as a proxy for general capturing on biosensing surfaces is far from being representative of all EV subpopulations, thus affecting sensitivy and also posing a bias towards EV based biomarker discovery projects. To overcome such issues, we speculate that further improvements will be lead by the use of pan-specific probes that provide unbiased EV capturing, like the recently introduced use of membrane sensing peptides (MSP) (Gori et al., 2020).

While crucial, sensitivity is not the only factor to be considered when evaluating analytical platform and many other important features such as throughput, time to result and multiplexing are worth to be carefully evaluated. A summary of the most peculiar traits for SP-IRIS and SiMoA platforms and associated instrumentations are summarised in Table 7.

4 | DISCUSSION

Although numerous systematic comparisons of EV analytical technologies have been published previously (Arab et al., 2021; Bachurski et al., 2019; Corso et al., 2019; Liang et al., 2021; Vogel et al., 2021), this work is, to the best of our knowledge, the first

TABLE 7 Summary of performances and peculiar traits of SP-IRIS and SiMoA platforms

	SP-IRIS	SiMoA
Operative detection range	$10^8 - 10^{10}$ EV/ml	$10^6 - 10^{10}$ EV/ml
Limit of Detection in spiking assay	10^8 EV/ml	10^7 EV/ml
Minimum Input volume	35 μl	125 μl (two steps assay) or 145 μl (three steps assay)
Reading time	Pre-scan: 12 min per chip (15 spots) + Post-scan: 12 min per chip (15 spots)	120 min per 96 well plate, 1,25 min per sample
Assay Operating Time	2.5 h sample incubation + 1 h secondary Ab + 20 total min washing	30 min sample/bead/secondary Ab incubation + 10 min SBG incubation +30 min total washing
Maximum Sample Multiplexing	16 samples per reading	96 samples per reading, 38 samples considering suggested replicates, controls and calibration
Antigen Multiplexing	5 positional and 3 detection channels	4 colour encodings available
Commercially available kits for EVs	Yes	No
Analysis Software dedicated to EV phenotyping	Yes	No
Additional information provided	Sizing, surface marker co-localisation, internal markers through permeabilisation assay	No

comparison of two digital detection platforms in immune-phenotyping of EVs. Specifically, this study evaluated the performance of SP-IRIS and SiMoA platforms in immunophenotyping of a well characterised EV sample from CPCs, focusing on the lower detection range. Notably, for the sake of a fair comparison, it makes use of the same immune-reagents (i.e., monoclonal antibodies against tetraspanins CD9, CD63, CD81) by customised functionalisation of the analytical supports (silicon chips for SP-IRIS and paramagnetic beads for SiMoA). A correlation of the techniques with Western Blotting could not be entirely assessed due to low detectability of CD81 in our conditions. In general, it is worth noticing that quantitative data from WB are difficult to attain, depending on the efficiency of many critical sequential steps including protein extraction, electrophoresis, transfer, immunodetection and imaging (Pillai-Kastoori et al., 2020). To correlate the limits of detection obtained by SP-IRIS and SiMoA assays with the relative abundance of CD9/CD63/CD81 a more quantitative technique such as Super Resolution Microscopy was used.

As far as sensitivity and operative range, under the conditions and settings we tested, SiMoA generally proved to be superior to SP-IRIS, in accordance with the recognised advantage of bead-based arrays as compared to flat microarrays. In line with this, while the low expression of CD81 in HeLa and CD63 in HEK was reflected in poor LODs for SP-IRIS, SiMoA was able to efficiently detect these low abundant species by overcoming one of the major bottleneck for sensitive detection in planar arrays which is mass-transport of analytes to surface-immobilised antibody. (Zhao et al., 2010)

Of note, when tested by the 'Needle-in-a-haystack' challenge of a mimicked liquid biopsy in complex sample, sensitivity of both platforms were affected, yet affording a remarkable LOD of 10^8 EV/ml for SP-IRIS and 10^7 EV/ml for SiMoA (Table 6). Inherently to the different assay format, the two platforms differ in minimum input volume of sample, which is lower in SP-IRIS, a remarkable advantage in many 'real life' applications and reading and operating time per sample which are generally shorter in SiMoA. In this frame, the level of automatisation of the assay and throughput is superior in SiMoA platform, where 96 versus 16 samples can be run simultaneously (Table 7). This consideration does not take into account recent upgrades of the Nanoview platform, which could not be tested here.

When CPC, HeLa and HEK EVs were analysed by Super Resolution Microscopy, their CD9/CD63/CD81 relative abundance appeared to be in very good accordance with the intensity of single-tetraspanin assay curves generated by SiMoA, whereas SP-IRIS failed, especially for the low abundant CD81, to represent such heterogeneity of expression.

Many other factors have to be taken into account when comparing the two technologies towards EV based biomarker discovery and their translation in clinics (Table 7). In this sense, the additional information provided by SP-IRIS platform in terms of label-free EV sizing, fluorescence co-localisation of biomarkers (Figure S3) and the availability of permeabilisation protocols to analyse

also luminal markers, make arguably this platform superior to SiMoA in biomarker discovery studies and competitive, for the wealth of information generated, with imaging and nano flow cytometry techniques. This reflects also in its dedicated software, well suited to straightforward and comprehensive EV analysis. On the other hand, when an established EV-based biomarker has to be analysed in many clinical samples with the highest sensitivity, as in biomarker validation projects, the total operating time and multiplexing capability of SiMoA are certainly appealing characteristics on the path for biomarker translation in clinic.

5 | CONCLUSIONS

Single molecule counting represents the highest achievable signal fidelity and perhaps the future of many analytical measurements will be based on single molecule detection and counting. Here we have compared, side by side, two commercially available digital instrumentations highly relevant to the EV field: the SP-IRIS and the SiMoA platform. A well characterized sample of human CPCs derived EVs was analysed and limits of detection (LODs), following different assay formats, were evaluated. A mimicked liquid biopsy assay provided a LOD of 10^8 EV/ml for the SP-IRIS and 10^7 EV/ml for the SiMoA platform. Considering sensitivity and detection range tested in this work and, more generally the throughput capability and level of automatisation, SiMoA seems to be the most suitable platform in clinical validation settings. On the other hand, due to the combination of label-free and fluorescence detection, SP-IRIS can return to users highly informative data on the analysed EV samples such as particle size and colocalisation of multiple external and internal biomarkers, making this platform the most appealing in research settings.

AUTHOR CONTRIBUTIONS
Alessandro Strada: Investigation; Methodology. Greta Bergamaschi: Investigation. Stefano Panella: Investigation. Cristina Grange: Investigation; Methodology. Marcello Marelli: Investigation. Gabriella Andriolo: Investigation. Benedetta Bussolati: Methodology; Writing – review & editing. Lucio Barile: Conceptualization; Methodology; Writing – review & editing. Marcella Chiari: Methodology. Alessandro Gori: Conceptualization; Funding acquisition; Methodology; Supervision; Writing – original draft; Writing – review & editing. Marina Cretich: Conceptualization; Funding acquisition; Methodology; Supervision; Writing – original draft; Writing – review & editing.

CONFLICT OF INTEREST
The authors declare no conflict of interests.

ORCID
Lucio Barile https://orcid.org/0000-0002-5827-0439
Marina Cretich https://orcid.org/0000-0001-8251-5275

REFERENCES
Andriolo, G., Provasi, E., Lo Cicero, V., Brambilla, A., Soncin, S., Torre, T., Milano, G., Biemmi, V., Vassalli, G., Turchetto, L., Barile, L., & Radrizzani, M. (2018). Exosomes from human cardiac progenitor cells for therapeutic applications: Development of a GMP-Grade Manufacturing Method. *Frontiers in Physiology*, *9*, 1169.

Arab, T., Mallick, E. R., Huang, Y., Dong, L., Liao, Z., Zhao, Z., Gololobova, O., Smith, B., Haughey, N. J., Pienta, K. J., Slusher, B. S., Tarwater, P. M., Tosar, J. P., Zivkovic, A. M., Vreeland, W. N., Paulaitis, M. E., & Witwer, K. W. (2021). Characterization of extracellular vesicles and synthetic nanoparticles with four orthogonal single particle analysis platforms. *Journal of Extracellular Vesicles*, *10*(6), e12079.

Bachurski, D., Schuldner, M., Nguyen, P. H., Malz, A., Reiners, K. S., Grenzi, P. C., Babatz, F., Schauss, A. C., Hansen, H. P., Hallek, M., & Pogge von Strandmann, E. (2019). Extracellular vesicle measurements with nanoparticle tracking analysis an accuracy and repeatability comparison between NanoSight NS300 and ZetaView. *Journal of Extracellular Vesicles*, *8*(1), 1596016.

Bordanaba-Florit, G., Royo, F., Kruglik, S. G., & Falcón-Pérez, J. M. (2021). Using single-vesicle technologies to unravel the heterogeneity of extracellular vesicles *Nature Protocols*, *16*(7), 3163–3185.

Campos-Silva, C., Suárez, H., Jara-Acevedo, R., Linares-Espinós, E., Martinez-Piñeiro, L., Yáñez-Mó, M., & Valés-Gómez, M. (2019). High sensitivity detection of extracellular vesicles immune-captured from urine by conventional flow cytometry. *Science Reports*, *9*(1), 2042.

Cavallaro, S., Hååg, P., Viktorsson, K., Krozer, A., Fogel, K., Lewensohn, R., Linnros, J., & Dev, A. (2021). Comparison and optimization of nanoscale extracellular vesicle imaging by scanning electron microscopy for accurate size-based profiling and morphological analysis. *Nanoscale Advances*, *3*(11), 3053–3063.

Cohen, L., & Walt, D. R. (2019). Highly Sensitive and Multiplexed Protein Measurements. *Chemical Reviews*, *119*, 293–321. https://doi.org/10.1021/acs.chemrev.8b00257

Corso, G., Heusermann, W., Trojer, D., Görgens, A., Steib, E., Voshol, J., Graff, A., Genoud, C., Lee, Y., Hean, J., Nordin, J. Z., Wiklander, O. P. B., El Andaloussi, S., & Meisner-Kober, N. (2019). Systematic characterization of extracellular vesicle sorting domains and quantification at the single molecule single vesicle level by fluorescence correlation spectroscopy and single particle imaging. *Journal of Extracellular Vesicles*, 8(1), 1663043.

Cretich, M., Daaboul, G. G., Sola, L., Ünlü, M. S., & Chiari, M. (2015). Digital detection of biomarkers assisted by nanoparticles: Application to diagnostics. *Trends in Biotechnology*, 33(6), 343–351.

Daaboul, G. G., Gagni, P., Benussi, L., Bettotti, P., Ciani, M., Cretich, M., Freedman, D. S., Ghidoni, R., Ozkumur, A. Y., Piotto, C., Prosperi, D., Santini, B., Ünlü, M. S., & Chiari, M. (2016). Digital detection of exosomes by interferometric imaging. *Science Reports*, 6, 37246.

Daaboul, G. G., Lopez, C. a., Chinnala, J., Goldberg, B. B., Connor, J. H., & Selim Ünlü, M. (2014). Digital sensing and sizing of vesicular stomatitis virus pseudotypes in complex media: A model for Ebola and Marburg detection. *ACS Nano*, 8, 6047–6055.

Dogrammatzis, C., Saleh, S., Deighan, C., & Kalamvoki, M. (2021). Diverse populations of extracellular vesicles with opposite functions during herpes simplex virus 1 infection. *Journal of Virology*, 95(6), e02357–20.

Frigerio, R., Musicò, A., Brucale, M., Ridolfi, A., Galbiati, S., Vago, R., Bergamaschi, G., Ferretti, A. M., Chiari, M., Valle, F., Gori, A., & Cretich, M. (2021). Extracellular vesicles analysis in the COVID-19 era: Insights on serum inactivation protocols towards downstream isolation and analysis. *Cells*, 10(3), 544.

Gori, A., Romanato, A., Bergamaschi, G., Strada, A., Gagni, P., Frigerio, R., Brambilla, D., Vago, R., Galbiati, S., Picciolini, S., Bedoni, M., Daaboul, G. G., Chiari, M., & Cretich, M. (2020). Membrane binding peptides for extracellular vesicles on chip analysis. *Journal of Extracellular Vesicles*, 9(1), 1751428.

Gorris, H. H., & Walt, D. R. (2010). Analytical chemistry on the Femtoliter Scale. *Angewandte Chemie International Edition*, 49, 3880–3895.

Hartjes, T., Mytnyk, S., Jenster, G., van Steijn, V., & van Royen, M. (2019). Extracellular vesicle quantification and characterization: Common methods and emerging approaches *Bioengineering*, 6(1), 7.

Hilton, S. H., & White, I. M. (2021). Advances in the analysis of single extracellular vesicles: A critical review. *Sensors and Actuators Reports*, 3, 100052. https://doi.org/10.1016/j.snr.2021.100052

Jeppesen, D. K., Fenix, A. M., Franklin, J. L., Higginbotham, J. N., Zhang, Q., & Zimmerman, L. J. (2019). Reassessment of Exosome Composition. *Cell*, 177, 428–445. e18. https://doi.org/10.1016/j.cell.2019.02.029

Johnsen, K. B., Gudbergsson, J. M., Andresen, T. L., & Simonsen, J. B. (2019). What is the blood concentration of extracellular vesicles? Implications for the use of extracellular vesicles as blood-borne biomarkers of cancer. *Biochimica et Biophysica Acta - Rev Cancer*, 1871(1), 109–116.

Kalluri, R., & LeBleu, V. S. (2020). The biology, function , and biomedical applications of exosomes *Science (80-.)*, 367(6478), eaau6977.

Khan, N. Z., Cao, T., He, J., Ritzel, R. M., Li, Y., Henry, R. J., Colson, C., Stoica, B. A., Faden, A. I., & Wu, J. (2021). Spinal cord injury alters microRNA and CD81+ exosome levels in plasma extracellular nanoparticles with neuroinflammatory potential. *Brain, Behavior, and Immunity*, 92, 165–183.

Li, J.-W., Shi, D., Wan, X.-C., Hu, J., Su, Y.-F., & Zeng, Y.-P. (2021). Universal extracellular vesicles and PD-L1+ extracellular vesicles detected by single molecule array technology as circulating biomarkers for diffuse large B cell lymphoma. *Oncoimmunology*, 10. https://doi.org/10.1080/2162402X.2021.1995166

Liang, Y., Lehrich, B. M., Zheng, S., & Lu, M. (2021). Emerging methods in biomarker identification for extracellular vesicle based liquid biopsy. *Journal of Extracellular Vesicles*, 10(7), e12090.

Liu, H., & Lei, Y. (2021). A critical review: Recent advances in digital biomolecule detection with single copy sensitivity. *Biosensors & Bioelectronics*, 177, 112901.

Min, L., Wang, B., Bao, H., Li, X., Zhao, L., Meng, J., & Wang, S. (2021). Advanced nanotechnologies for extracellular vesicle based liquid biopsy. *Advancement of Science*, 2102789.

Mizenko, R. R., Brostoff, T., Rojalin, T., Koster, H. J., Swindell, H. S., Leiserowitz, G. S., Wang, A., & Carney, R. P. (2021). Tetraspanins are unevenly distributed across single extracellular vesicles and bias sensitivity to multiplexed cancer biomarkers. *Journal of Nanobiotechnology*, 19(1), 250.

Montis, C., Zendrini, A., Valle, F., Busatto, S., Paolini, L., Radeghieri, A., Salvatore, A., Berti, D., & Bergese, P. (2017). Size distribution of extracellular vesicles by optical correlation techniques. *Colloids Surfaces B Biointerfaces*, 158, 331–338.

Morasso, C., Ricciardi, A., Sproviero, D., Truffi, M., Albasini, S., & Piccotti, F. (2022). Fast quantification of extracellular vesicles levels in early breast cancer patients by Single Molecule Detection Array (SiMoA). *Breast Cancer Research and Treatment*, 192, 65–74. https://doi.org/10.1007/s10549-021-06474-3

Norman, M., Ter-Ovanesyan, D., Trieu, W., Lazarovits, R., Kowal, E. J. K., Lee, J. H., Chen-Plotkin, A. S., Regev, A., Church, G. M., & Walt, D. R. (2021). L1CAM is not associated with extracellular vesicles in human cerebrospinal fluid or plasma. *Nature Methods*, 18(6), 631–634.

Pillai-Kastoori, L., Schutz-Geschwender, A. R., & Harford, J. A. (2020). A systematic approach to quantitative Western blot analysis. *Analytical Biochemistry*, 593, 113608.

Rissin, D. M., Kan, C. W., Campbell, T. G., Howes, S. C., Fournier, D. R., Song, L., Piech, T., Patel, P. P., Chang, L., Rivnak, A. J., Ferrell, E. P., Randall, J. D., Provuncher, G. K., Walt, D. R., & Duffy, D. C. (2010). Single-molecule enzyme-linked immunosorbent assay detects serum proteins at subfemtomolar concentrations. *Nature Biotechnology*, 28(6), 595–599.

Skovronova, R., Grange, C., Dimuccio, V., Deregibus, M. C., Camussi, G., & Bussolati, B. (2021). Surface marker expression in small and medium/large mesenchymal stromal cell-derived extracellular vesicles in naive or apoptotic condition using orthogonal techniques. *Cells*, 10(11), 2948.

Ter-Ovanesyan, D., Norman, M., Lazarovits, R., Trieu, W., Lee, J.-H., Church, G. M., & Walt, D. R. (2021). Framework for rapid comparison of extracellular vesicle isolation methods. *Elife*, 10, e70725.

Théry, C., Witwer, K. W., Aikawa, E., Alcaraz, M. J., Anderson, J. D., Andriantsitohaina, R., Antoniou, A., Arab, T., Archer, F., Atkin-Smith, G. K., Ayre, D. C., Bach, J.-M. M., Bachurski, D., Baharvand, H., Balaj, L., Baldacchino, S., Bauer, N. N., Baxter, A. A., Bebawy, M., & Zuba-Surma, E. K. (2018). Minimal information for studies of extracellular vesicles 2018 (MISEV2018): A position statement of the International Society for Extracellular Vesicles and update of the MISEV2014 guidelines. *Journal of Extracellular Vesicles*, 7(1), 1535750.

Tian, Y., Gong, M., Hu, Y., Liu, H., Zhang, W., Zhang, M., Hu, X., Aubert, D., Zhu, S., Wu, L., & Yan, X. (2020). Quality and efficiency assessment of six extracellular vesicle isolation methods by nano flow cytometry. *Journal of Extracellular Vesicles*, 9(1), 1697028.

van der Pol, E., Coumans, F. A. W., Grootemaat, A. E., Gardiner, C., Sargent, I. L., Harrison, P., Sturk, A., van Leeuwen, T. G., & Nieuwland, R. (2014). Particle size distribution of exosomes and microvesicles determined by transmission electron microscopy, flow cytometry, nanoparticle tracking analysis, and resistive pulse sensing. *Journal of Thrombosis and Haemostasis*, 12(7), 1182–1192.

Vogel, R., Savage, J., Muzard, J., Della Camera, G., Vella, G., Law, A., Marchioni, M., Mehn, D., Geiss, O., Peacock, B., Aubert, D., Calzolai, L., Caputo, F., & Prina-Mello, A. (2021). Measuring particle concentration of multimodal synthetic reference materials and extracellular vesicles with orthogonal techniques: Who is up to the challenge? *Journal of Extracellular Vesicles*, 10(3), e12052.

Wei, P., Wu, F., Kang, B., Sun, X., Heskia, F., Pachot, A., Liang, J., & Li, D. (2020). Plasma extracellular vesicles detected by Single Molecule array technology as a liquid biopsy for colorectal cancer. *Journal of Extracellular Vesicles*, 9(1), 1809765.

Welsh, J. A., Pol, E., Bettin, B. A., Carter, D. R. F., Hendrix, A., Lenassi, M., Langlois, M., Llorente, A., Nes, A. S., Nieuwland, R., Tang, V., Wang, L., Witwer, K. W., & Jones, J. C. (2020). Towards defining reference materials for measuring extracellular vesicle refractive index, epitope abundance, size and concentration. *Journal of Extracellular Vesicles*, 9(1), 1816641.

Yates, A. G., Pink, R. C., Erdbrügger, U., Siljander, P. R., Dellar, E. R., & Pantazi, P. (2022). In sickness and in health: The functional role of extracellular vesicles in physiology and pathology in vivo. *Journal of Extracellular Vesicles*, *11*. https://doi.org/10.1002/jev2.12151

Yoshioka, Y., Konishi, Y., Kosaka, N., Katsuda, T., Kato, T., & Ochiya, T. (2013). Comparative marker analysis of extracellular vesicles in different human cancer types. *Journal of Extracellular Vesicles*, *2*(1), 20424.

Yurt, A., Daaboul, G. G., Connor, J. H., Goldberg, B. B., & Selim Ünlü, M. (2021). Single nanoparticle detectors for biological applications. *Nanoscale*, *4*, 715.

Zhao, M., Wang, X., & Nolte, D. (2010). Prostate specific antigen detection in patient sera by fluorescence-free BioCD protein array. *Analytical Biochemistry*, *1*(3), 442–453.

SUPPORTING INFORMATION

Additional supporting information can be found online in the Supporting Information section at the end of this article.

How to cite this article: Frigerio, R., Musicò, A., Strada, A., Bergamaschi, G., Panella, S., Grange, C., Marelli, M., Ferretti, A. M., Andriolo, G., Bussolati, B., Barile, L., Chiari, M., Gori, A., & Cretich, M. (2022). Comparing digital detection platforms in high sensitivity immune-phenotyping of extracellular vesicles. *Journal of Extracellular Biology*, *1*, e53. https://doi.org/10.1002/jex2.53